



Digital image correlation (DIC) for measurement of strains and displacements in coarse, low volume-fraction FRP composites used in civil infrastructure



Enrique del Rey Castillo^{a,*}, Tom Allen^b, Richard Henry^a, Michael Griffith^c, Jason Ingham^a

^a Dept. of Civil and Environmental Engineering, The University of Auckland, New Zealand

^b Center for Advanced Composite Materials (CACM), Mechanical Engineering Dept., The University of Auckland, New Zealand

^c School of Civil, Environmental and Mining Engineering, University of Adelaide, Australia

ARTICLE INFO

Keywords:

DIC
FRP
Strain fields
Bond
FRP anchors
Strengthening

ABSTRACT

Accurately measured strains are critical when investigating the application of Fiber Reinforced Polymer (FRP) materials, but traditional mechanical strain measurement methods have several critical drawbacks related to the installation process and the recording capabilities of the devices. FRP materials typically used in the civil engineering field feature large asymmetries and heterogeneity originated from the manual installation procedures, as opposed to the highly controlled FRP fabrication methods used in other fields that result in more homogeneous materials. The feasibility of using an optical full-field Digital Image Correlation (DIC) technique for measurement of strain fields on FRP materials used in the civil engineering industry has been investigated and the level of error in the DIC method when using more traditional methods was determined. The main advantage of using DIC over more traditional methods, which is the capacity of DIC to measure full field strains instead of strains at isolated points, has been demonstrated by providing exemplar measurements of various specimens of FRP materials. The reported strain fields are examples of what was obtained during an experimental campaign to understand the behavior of FRP anchors and other materials. The main conclusions drawn from the observation of those strain fields are discussed.

1. Introduction

Determining operational limits and safe working strains, as identified in international guidelines such as ACI 440.2R [1] and CNR-DT 200 [2], is paramount to the application of Fiber Reinforced Polymers (FRP) in civil engineering. One of the most common applications of FRP materials in civil engineering is as Externally Bonded Reinforcement systems (EBR-FRP) to strengthen existing structures. Accurate measurement of the FRP strains when under load in such applications provides insight and understanding of the load distribution within the FRP material. When conducting tests, a number of traditional instruments are available for the measurement of displacements and strains, including Linear Variable Differential Transformer devices (LVDT) or foil Strain Gauges (SG). These instruments have been in use for decades, but feature some significant drawbacks as the installation of the instrumentation is typically invasive, expensive, cumbersome or time-consuming. But the most significant deficiency of these devices is that they only measure displacements or strains at specific, isolated points.

Spatial strain fields allow both general strain distributions and localized strain concentrations to be observed. Spatial strain field measurements are critical when investigating EBR-FRP systems, where the FRP materials are non-homogenous and highly anisotropic as opposed to more traditional metallic or cementitious materials. This effect is exacerbated by “low-tech” in situ manufacturing methodologies typically involved in the installation of EBR-FRP systems. The manufacturing approaches typically used in EBR-FRP systems result in low fiber volume fractions, which is defined as the ratio between the volume of fibers and the total volume, and in large variations in fiber orientation both in-plane and through thickness due to the lack of molding/compression force. Modern full-field imaging techniques such as Digital Image Correlation (DIC), thermograph and particle image velocimetry enable the determination of strain fields during testing. Full-field digital imaging techniques are increasing in availability and are frequently applied to composite structures [3,4], however to date much of the research of digital imaging techniques in composites has been focused on high-end composites manufactured using resin infusion, resin transfer moulding

* Corresponding author.

E-mail address: edel146@aucklanduni.ac.nz (E. del Rey Castillo).

<https://doi.org/10.1016/j.compstruct.2019.01.024>

Received 29 October 2018; Received in revised form 5 December 2018; Accepted 2 January 2019

Available online 04 January 2019

0263-8223/ © 2019 Elsevier Ltd. All rights reserved.

or pre-impregnated textiles. The materials addressed in this work present novel challenges in that the surface of the structure has significant undulations, with large local stiffness variations due to the low volume fraction and the frequent misalignment of fiber orientation as a result of the on-site installation process. The validation and application of a Digital Image Correlation methodology to coarse, low fiber-volume fraction FRP materials is presented, together with examples of the results that can be obtained and how to interpret them.

1.1. Digital Image Correlation fundamentals, spherical lens aberration and 3D image rectification

Digital Image Correlation (DIC) involves the calculation of displacements and material strains by tracking the movement of features in consecutive images and was firstly developed in the 1980s at a time when digital cameras and powerful computers were scarce and expensive if available at all [5]. Several computer programs appeared in an attempt to solve the high computational load that characterized the first attempts to use DIC [6], and continuous efforts have been made to improve the efficiency and the accuracy of DIC through different algorithms and computational tools [7,8].

DIC can be used to record displacements and transform them into strains at isolated points (typically known as virtual gauges) or to obtain full field displacement or strain maps. Full field strain maps are remarkably useful when studying the behavior of FRP materials, due to the complexity of these materials and the influence of concentration of localized strains in the behavior. DIC can be used in a two-dimensional (2D) configuration, which requires only one camera, or in a three-dimensional (3D) configuration, which requires the use of two cameras on the same field of view and a more complex processing. A wide range of DIC applications can be found in the literature, like material characterization through tension, compression, fatigue or shear testing [9], cyclic/fatigue testing of epoxy resins [10], identification of delamination on carbon FRP beams [11] and measurement the effect of impacts [12] or blasts [13] on metal, amongst others.

Two errors originated by the optical effects of the lens can affect the quality of the readings [14]. Lens spherical aberration is an optical effect that is inevitable when using lenses, as this effect occurs due to the refraction of the light rays passing through the camera lens and can appear in both 2D and 3D DIC techniques. The theory of spherical aberration, how to correct the distortion and examples of the verification of the correction can be found in the literature [15–17]. The second optical error is exclusive to 3D DIC, as this error is the result of projecting – or rectifying – two or more images onto a single plane image. The theory of combining two images to create a three-dimensional model was developed in the 80s and 90s [18], and different methods for 3D reconstruction have been developed in the past [19]. Sutton [7] compiled a thorough review on the effect of out of plane motion on 2D and 3D DIC readings, comparing CCD and telecentric cameras. No example could be found in the literature on the extent of 2D spherical aberration and 3D image rectification errors that can be expected when inexpensive DSLR cameras and variable focal length lenses are used, with different focal lengths and distance from specimen to camera are used. Furthermore, the influence of the ratio between calibration checkerboard size and field of view and of the number of tracking points on the correction of the distortion error have only been partially investigated to date [20].

A speckle pattern proportional to the specimen size and to the field of view needs to be produced into the specimen to obtain correct measurements, with multiple examples being available in the literature [21–24] and a thorough study being undertaken by Lecompt et al. [25]. For the current research, four different patterns were used until the correct one was found, but no further work is reported in this regard.

1.2. The use of DIC on FRP materials

DIC has been used extensively in the civil engineering industry, albeit mostly to track displacements, deflections or to identify the presence of cracks in reinforced concrete or masonry structures [26–29]. Many examples exist on the use of DIC to detect and study the bond behavior between FRP and substrate, both when the substrate is concrete [30,31,3] and masonry [32,33,4]. DIC has been typically used in the civil engineering field to measure displacement and strain at isolated points but strain fields were not obtained, which means that one of the most advantageous features of DIC technique was not exploited [34,35]. Multiple examples exist of full field displacement or strain measurements on FRP materials with DIC outside of the civil engineering field [36–42] but no studies could be found on the use of DIC to study in detail the type of FRP material used in the civil engineering field when fiber rupture failure mode is present.

Only one example could be found in the literature where full field displacement and strains were produced to investigate the behavior of FRP materials in a situation comparable to a real case use of FRP in civil engineering [43]. Full field strains of FRP reinforcement on an RC beam were obtained in the aforementioned study, to measure the overall FRP-RC composite behavior rather the detailed behavior of the FRP. Two strain gauges and two LVDTs at isolated points were used to validate the data obtained with DIC, but not enough data was obtained to have a conclusive validation.

A few attempts have been undertaken to validate the use of DIC measurements with alternative equipment. A few examples exist where DIC (2D and 3D) and a discrete number of foil strain gauges were used to validate strains [44,36,45,38,46,20], but in some cases the information regarding the foil strain gauges properties is incomplete, or the foil strain gauges and the virtual strain gauges were placed at different points, compromising a direct comparison between DIC and SGs. Mehdikhani [24] used FEM models to calibrate the displacements and strains obtained on virtually deformed and microscopically obtained images of FRP materials, but the microscopic scale of the work compromises the validity when large scale testing is involved. Ivanov [39] also used FEM to validate DIC readings, but the authors could not achieve a correspondence between FEM and DIC. Tekieli [4] compared the readings from an extensometer and 2D DIC on several FRP substrates, and produced full field strains to detect cracks and FRP-to-substrate debonding, but not to obtain strains at rupture.

1.3. Research motivation

Full strain fields are crucial to understand and model the behavior of FRP materials, and DIC gives researchers the opportunity to obtain them. The main objective of the research reported herein is to give examples of the readings that can be obtained with DIC on FRP materials for different specimen sizes and uses, especially when fiber rupture failure mode is expected. How these results were used to understand the behavior of FRP materials in the civil engineering industry, especially focusing to understand fibre rupture mechanisms, is discussed in detail.

The motivation of the research was double, first to assess the accuracy of using DIC in combination with inexpensive and easy to use DSLR cameras to obtain full strain fields with FRP materials, and second to report and discuss the results that can be obtained when the rupture of the fibers is expected, particularly when a heterogeneous FRP material with resin- and fiber-rich areas is used.

2. Experimental program

The material morphology, testing test set-ups and methodology is described in this section, together with the verification of the error that can be expected when using DIC with the FRP materials used in the civil engineering field.

2.1. Material morphology

Material homogeneity and surface topology have significant influence on the surface strains of a material under stress but the majority of existing research utilizing DIC on composite structures has been on marine or aerospace composites. In these fields the FRP manufacturing methods are highly controlled processes which result in homogeneous and consistent materials and typically involve multi-directional weaves. These material systems are typically characterized by a high fiber volume fraction (also known as fiber volume ratio), which is the percentage of fiber volume in the entire volume of the FRP composite material. However, in the civil industry the installation usually takes place in the construction site using unidirectional fabric and an unconsolidated wet-layup process with highly dependence on the quality of workmanship [47], in contrast to the closed molded or vacuum bagged processes typically used in higher end composite structures.

While the fiber volume ratio is typically 50% or even higher when controlled manufacturing methods are involved, the ratio drops to 30% or even lower when the material is installed on site. The result of this manufacturing approach is a highly variable, heterogeneous and inconsistent composite that typically includes large spatial variations and a high level of surface undulation. These undulations consist of areas that are more fiber-rich and other areas that are more resin-rich, which can lead to three dimensional deformations even when three dimensional displacements are not expected. The difference in cross-section morphology between materials manufactured using a range of manufacturing methods is illustrated in Fig. 1. Composites manufactured using an autoclave pre-impregnated material is the most homogeneous with little variation through thickness and little to no voids, as can be seen in Fig. 1a. Resin infusion produces a slightly less homogeneous material and a higher number of voids as reported in Fig. 1b, however lower voids and more homogeneous than wet-hand laid materials as per Fig. 1c, as considered in this work.

This inherent variation resulting from the low technology manufacturing process leads to larger local variations in strain. Understanding the ability of full field imaging techniques to account for this variation and identify local areas of high stress/strain is important for developing insight into prediction of failure and initiation within industrial composites for civil applications.

2.2. Test set up and methodology

Two DSLR cameras with a graphic resolution of 24.3 megapixels and a lens with a focal distance of between 18 mm and 55 mm were used to acquire the images in RAW mode, placing them as close to each other as possible with constant and neutral white LED lights. Manual mode was used, adjusting the ISO, focal aperture and shutter speed to obtain the sharpest possible image but within the limits of: ISO between 100 and 250, focal aperture between 1/4.5 and 1/5.5 and shutter speed between 1/60 s and 1/100 s. The physical distance between the cameras was maintained at 300 mm, but the distance from the cameras to the specimen varied depending on the type of specimen used. The load data acquisition started at the exact moment at which the first image

was taken, which makes that first image as “zero” or non-loaded image. From that point the load and the image capturing process, and therefore the strain data, were synchronized.

DIC was used in a range of specimens of different sizes as part of a testing campaign to help understand the fibre rupture failure mode of FRP anchors, although all the results discussed herein are novel materials [48–57]. FRP tensile coupons 25 mm wide and between 150 mm and 200 mm were used to obtain the tensile properties of the FRP according to ASTM D3039 [58]. Foil strain gauges that were 5 mm long and 2 mm wide (FLA-5-11-1L from Tokyo Sokki Kenkyujo Ltd.) were used to measure strains on the FRP coupons and corroborate the strains measured with DIC. Two FRP coupons bonded using lap joints were used to investigate the FRP-to-FRP bond mechanism and strength, with the dimensions being in accordance with ASTM D5868 [59] and ASTM D3528 [60] for single and double lap joints respectively. FRP anchors are typically used to ensure the continuity of the load path from FRP sheets into the structure, and consist of a bundle of fibers that is introduced into the structure on one end and splayed to form a fan on the other end, which is then bonded onto the FRP sheet using epoxy resin [56]. Schematic examples of how FRP anchors are used are illustrated in Fig. 2 [61]. DIC was used in a wide range of FRP anchor testing to investigate the fibre rupture failure mechanism and develop a predictive model to calculate the anchor tensile capacity. Displacement gauges were installed on the outside of the FRP anchor to prevent any damage to the fibers, and the recordings from DIC were compared with the displacements obtained with the displacement gauges. Finally, DIC was used on FRP anchors incorporated into reinforced column seismic testing to capture at which point the fibers ruptured and in which manner. The observations from the use of DIC in all these situations is discussed in detail in Section 3 Results of DIC on FRP materials.

A speckle pattern on the specimen surface has been shown to have an influence on the reliability of the displacement and strain measurements [62]. A preliminary investigation was conducted to identify the most suitable speckle pattern to use. Four different patterns were tested; (a) as-is, (b) sandpapering the surface to eliminate the glossy finishing and reflections, (c) with white dots painted with a marker, and (d) spray-painting the specimen with two layers, which gave the best results of all and was used in all consequent tests. The spray-painting pattern consisted of a first black matte layer to eliminate reflections and then a second white layer sprayed from a distance in short bursts to obtain small droplets on the specimen surface that would produce the irregular pattern, examples are provided in Fig. 3. The spray-painting pattern resulted in the speckles having a pixel size of between 3×3 pixels or 4×4 pixels. More details regarding speckle properties and influence on the readings can be found in the literature [23,24].

TRIDENT V3.0, an image processing Matlab [63] GUI developed by the Centre for Advanced Composite Materials (CACM) at the University of Auckland, was used to obtain the DIC results in this research. It is important to note that DIC systems can be purchased on the market and that DIC analyzing software can be freely downloaded from the internet. Details of the TRIDENT V3.0 tracking algorithms and implementation are presented by Stubbing [64], who has subsequently developed its 3D strain field capabilities [65]. The parameters used for

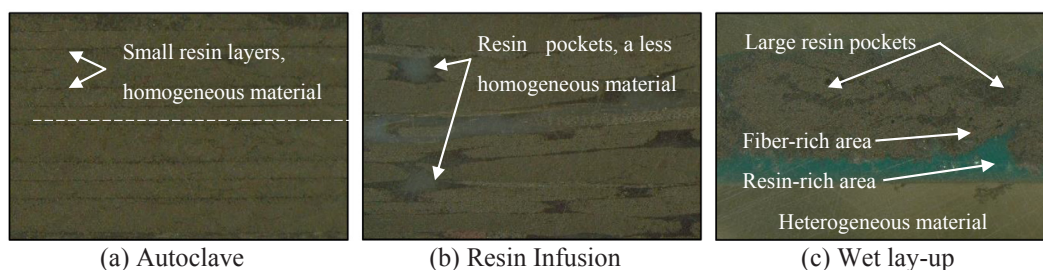


Fig. 1. Comparison of cross-section morphology of composites using different manufacturing methods.

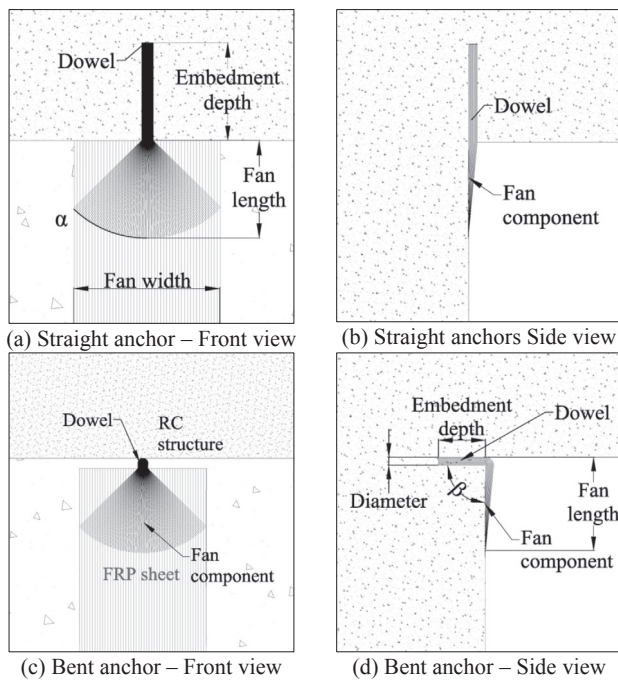


Fig. 2. Attributes of FRP anchors.

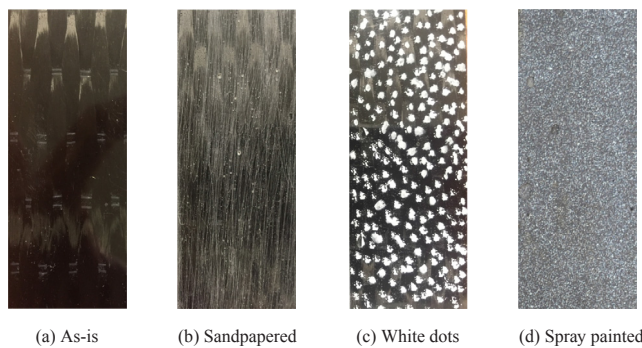


Fig. 3. Four different surface treatments under study.

Table 1
DIC details.

Parameters used for analysis of images		Optical system components	
Subset size	15 × 15 pixels ²	Cameras	Nikon D5600
Step size	15 pixels	Lenses	Nikon 18–55 mm f/3.5–5.6G DX VR
Shape function	Cubic	Lighting	White LED lighting
Strain filter size	15 × 15	Environment	Laboratory conditions (15–25°C)

analysis of images are reported in Table 1.

To record strains and maximize the benefit of TRIDENT’s sub-pixel resolution a fine speckle pattern was required, with a speckle size between four and sixteen pixels. The as-is, white dots and sandpapered surfaces (Fig. 3) gave poor results due to the speckle pattern coarseness whereas the spray painted surface treatment (Fig. 3d) provided the greatest number of high-contrast features for the software to track.

2.3. Test matrix

An overview of the test program is presented in Table 2, where each tested specimen is listed together with the properties of the tested specimen, the objective of the test, and the subsequent section and

Figure where the results are discussed. As can be inferred from Table 2, the two main objectives of the research (verification of the technique and report of the typical results that can be obtained) overlapped towards the middle of the testing program.

2.4. Reprojection error

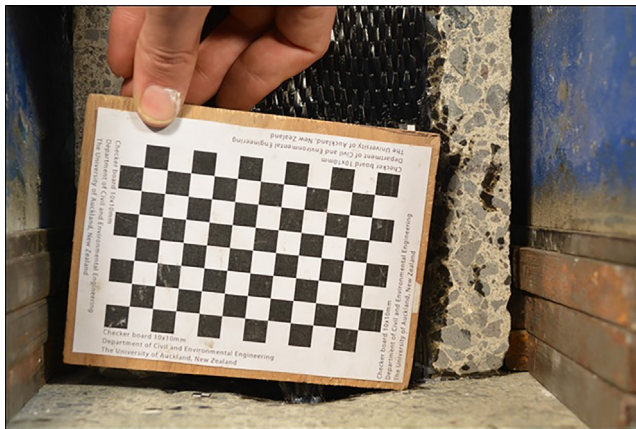
A lens spherical aberration calibration process was conducted as the first step using Bouguet’s toolbox [66] based on the Heikkilä and Silvén method [67] to identify the range of reprojection error expected when using DIC on small scale FRP anchors. This section describes the error that can be expected when DSLR cameras are used, given that the distortion and quality of the images obtained with these cameras is significantly reduced when compared with the images obtained with the typically used CCD and telecentric cameras. The reprojection error is described as the distance between any given points in the image to where that point is. Two main sources may exist for having a large reprojection error, i) the spherical aberration caused by the lens and ii) errors between the mathematical camera model and the physical camera behavior. The calibration process was thoroughly described by Yang et al. [27]. To perform the calibration correctly between 10 and 12 photos of checkerboards of different sizes were taken, in which the exact dimension of the black and white squares were known. As an example, the checkerboard in Fig. 4 features squares with dimensions of 10x10 mm.

Three checkerboards with the same number of squares but different square sizes of 10 × 10 mm, 15 × 15 mm and 20 × 20 mm were used, which corresponds approximately to 125, 175 and 225 pixels respectively. By maintaining the same number of squares but increasing their size the overall size of the checkerboard increased. The checkerboard sizes under investigation were approximately half, a quarter and an eighth of the size of the field of view, with the cameras being installed at three distances from the specimen but maintaining the same field of view. At least ten sharp and properly illuminated photos were taken, ensuring that the field of view edges were covered. The three distances were as close to the specimen as possible with a focal length of 18 mm, at medium range with a focal length of 35 mm, and as far away from the specimen as possible with a focal length of 55 mm. The objective was to compare the spherical aberration that the lens would produce when studying the same specimen from different distance and changing the focal length to maintain the field of view. Although a fixed focal length lens would reduce the likelihood of introducing errors due to the difficulty to repeat the exact same focal length of 35 mm, a variable focal length lens was favored because the versatility of having different focal lengths within the same equipment. The reprojection error resulted as a correction of the lens spherical aberration was small as can be seen in Fig. 5. For all checkerboard sizes and camera locations the reprojection error was less than 0.056 pixels, with the largest error being obtained when a checkerboard half the side of the field of view was used. The reprojection error produced by lens spherical aberration was measured using the Camera Calibrator application included in the Computer Vision System toolbox from Matlab [63]. The smallest reprojection error of 0.022 was obtained with a focal length of 35 mm at medium range, using a checkerboard a fourth or an eighth the size of the field of view, which was the configuration selected for all future tests. The average reprojection error was 0.036 pixels. The lens spherical aberration is typically smaller as the focal length increases, which would imply that the smallest spherical aberration is to be expected with a focal length of 55 mm. However, since the objective was to maintain constant field of view, the spherical aberration was also influenced by the distance from the specimen to the camera, hence the smallest lens spherical aberration and image rectification error being obtained with a focal length of approximately 35 mm.

A second calibration phase was undertaken using checkerboards featuring squares of the same size but different numbers of squares in each checkerboard. Tracking points are defined as the point where four

Table 2
DIC details.

	Verification of results		Strain fields results		Section (Figure)
	Characteristics	Objective	Characteristics	Objective	
D1 D2	Anchor testing with displacement gauges	Verify accuracy of DIC displacements	–	–	2.5 8
S1 S2	FRP coupon test with single foil strain gauge in the direction of loading	Verify strain accuracy in direction parallel to fibers and load	–	–	2.6 9
M1 M2	FRP coupon test with multiple foil strain gauges in multiple directions	Verify strain accuracy in multiple directions	Coupon subjected to unidirectional tensile load	Verify the strain uniformity in orthogonal directions	2.6 10 3.1 11 1213
L	–	–	Tensile coupon with single lap splice	Determine the lap splice strength	3.1 14
A1 A2 A3	–	–	A narrow straight anchor A wide bent anchor A wide straight anchor	Study load path, failure mechanism, capacity and develop a predictive model	3.2 1516 17
C	–	–	Anchors installed at the column-foundation joint	Predictive model verification in full scale structural elements	3.3 18

**Fig. 4.** Example of a calibration checkerboard.

squares meet, excluding the outer line of points, such that for example the checkerboard in Fig. 4 shows $11 \times 7 = 77$ tracking points. The number of tracking points for the 3 checkerboards were 15, 77 and 345, with the results when using 77 tracking points being the most accurate of the three configurations as can be seen in Fig. 6. The reprojection error was negligible, being approximately 0.042 pixels in average. The reprojection error obtained indicates that 2D DIC using DSLR cameras, without compensating for reprojection error, is accurate enough to measure displacements and strains on FRP materials as used in the civil engineering industry, although the process of calibrating the reprojection error certainly increases the accuracy of the recordings. The negligible reprojection error also indicated a good match between the mathematical camera model and the actual/physical camera behavior.

2.5. Verification of displacements

Two FRP anchor specimens (D1 and D2) were used to verify the accuracy and reliability of the displacements measured with DIC by installing displacement gauges close to the targets used for DIC as reported in Fig. 7. Note that there are six targets in Fig. 7, four next to the anchor (two of them highlighted in yellow) and two on the floor that are barely visible in the figure but that did not move during testing. The distance between targets and between displacement gauges is approximately 55 mm. A comparison between the DIC and displacement

gauges is shown in Fig. 8 for both FRP anchor specimens. The maximum difference corresponds to 0.2 mm (around photo number 21 of Fig. 8b), but this difference is most probably related to the displacement gauges rather than the readings from the cameras, as indicated by the rise in the black curve. The displacement at peak was significantly smaller, with a difference of 0.05 and 0.07 mm corresponding to 2.8% and 1.4% respectively. This difference is somewhat smaller than previous observations, where a typical measurement difference between 4% and 6% has been observed, peaking at 10% difference [29].

2.6. Verification of strains

FRP coupon specimens were tested in general accordance with ASTM D3039 [58]. Specimens S1 and S2 had a single foil strain gauge (aligned with the direction of loading) placed centrally on one face of the specimen, while a spray paint surface treatment was applied to the other face for DIC to be used. The strains, recorded parallel to the load and fibers for both specimens, are reported in Fig. 9. The solid line is the strain from the SG, which is 5 mm long, while the dashed line is the result calculated from the DIC, calculated with a subset size of 15 pixels. The DIC result was calculated as the average strain measured over an area that was equal to and located directly opposing the foil strain gauge. Photos were taken every 10 s for specimen S1 (67 photos) and every 3 s for specimen S2 (385 photos), while maintaining the loading rate constant for both specimens (0.01 mm/s). The DIC data was correlated with the applied load values by synchronizing the start of the test with the first photo without applied load, which was numbered as photo number 0 in the post-processing and in Figs. 9–11.

The strain fields in the direction longitudinal to the fibers (ϵ_l) obtained from DIC for specimen S2 at loads of 7, 14 and 21 kN are presented in Fig. 9. Due to the weave of the FRP textile used in the coupon the fiber tows have some out-of-plane crimp, rather than being completely straight. As the load and therefore longitudinal strains increased the variation in local strains as a result of the tow crimp became more visible in the DIC strain fields. The correlation between the results recorded with DIC and with SG supports the use of DIC to measure strains in the direction parallel to the fiber. Furthermore, the strain fields presented in Fig. 9 indicate the ability of DIC to satisfactorily measure local strain variations, with a maximum difference between the reading obtained with DIC and with SG of 0.06%.

Further testing was undertaken, with multiple foil strain gauges placed at different locations and in different directions. SGs were

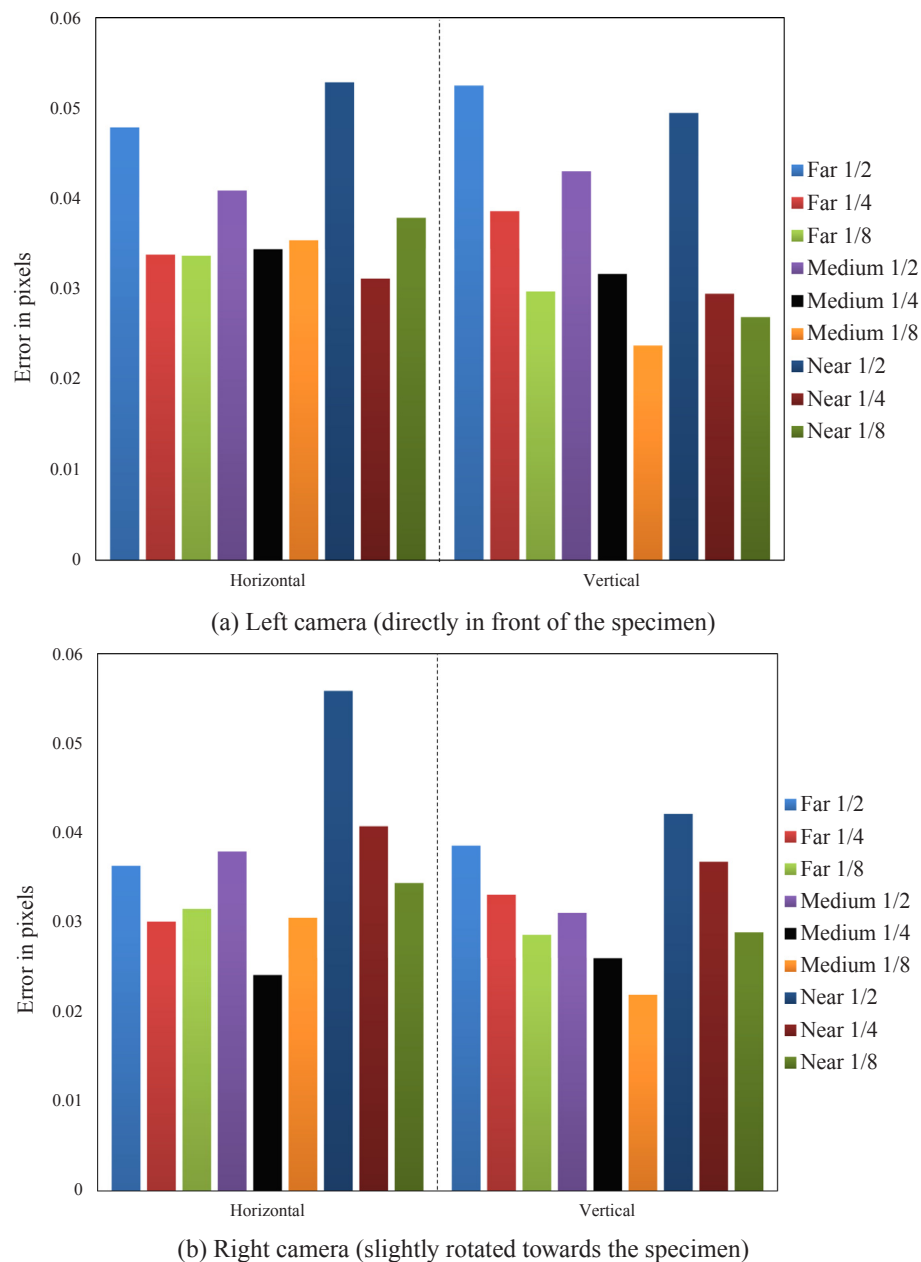


Fig. 5. Reprojection error depending on camera position and the ratio between checkerboard size and frame size.

installed on specimens M1 and M2 at the locations detailed in Figs. 10 and 11 respectively. DIC was again used to determine the strain field on the opposing face to the foil strain gauges. The DIC measurements were calculated following the same procedure as for specimens S1 and S2, over an area that matched the same size and location as each of the foil strain gauges. For SG4, SG5 and SG6 a square including all three foil strain gauges was selected. Photos were taken every 5 s for M1 (158 photos) and every 4 s for M2 (184 photos). A good correlation was observed for the strains recorded in the direction parallel to the fiber (SG1, SG3, SG4, SG7 and SG9), similar to the results obtained for specimens S1 and S2. The strains in the transverse direction (SG2, SG6 and SG8) recorded with foil strain gauges were consistently lower than those recorded with DIC. The SGs were installed transverse to the fiber tows and, given that the SGs were longer than the width of one fiber tow, the recorded strains were the average of the strains from several adjacent fiber tows. This effect leads to inconsistencies in the strain readings, for both the SGs and DIC. The solution to solve or minimize the divergent reading could be to limit the recordings to a single tow

but this possibility does not exist with SGs because of their size. SG5 recorded the strain in the XY direction, which for DIC was obtained by rotating the image 45 degrees. The foil strain gauges recorded sudden jumps at different moments during the test, or stopped altogether, likely due to debonding of the foil strain gauge from the FRP coupon.

A second specimen with multiple foil strain gauges was tested (M2), with the results being consistent with those from M1 as can be seen in Fig. 11. The correlation was good for longitudinal strains (SG2, SG3, SG4, SG7 and SG9) but poor for transverse strains (SG1, SG6, and SG8) and for strains in the XY direction (SG5). The problem of the SGs debonding from the FRP coupon was partially corrected with a more careful installation process in specimen M2 when compared to specimen M1, where all the SGs stopped recording at approximately step number 138. The surface was more meticulously cleaned with acetone previous to installation of the SGs and a different type of glue recommended by the SG manufacturer was used on specimen M2. DIC did not experience the debonding problem in any of the experiments, thereby proving to be a more reliable method to measure strains than is

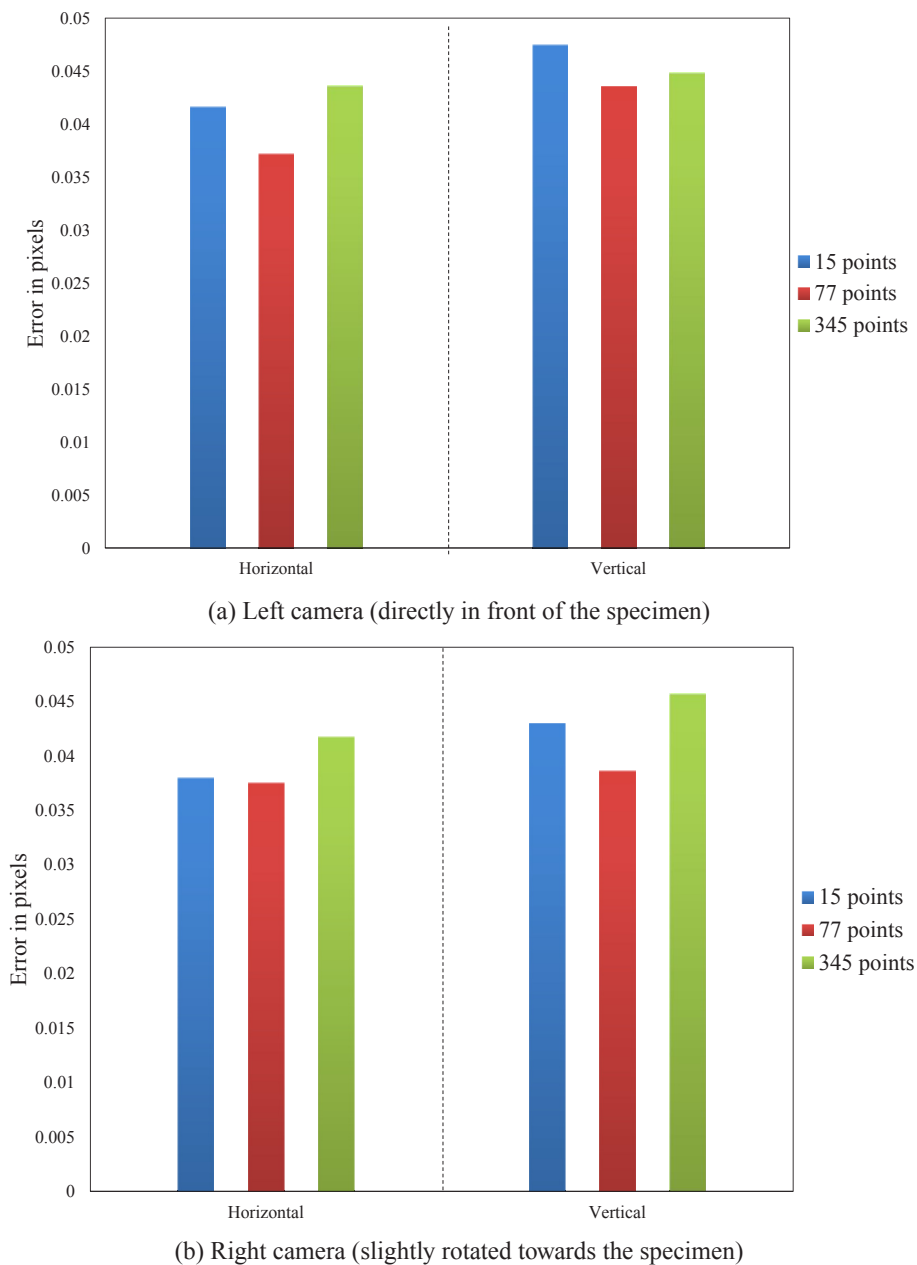


Fig. 6. Reprojection error depending on number of tracking points in a checkerboard.

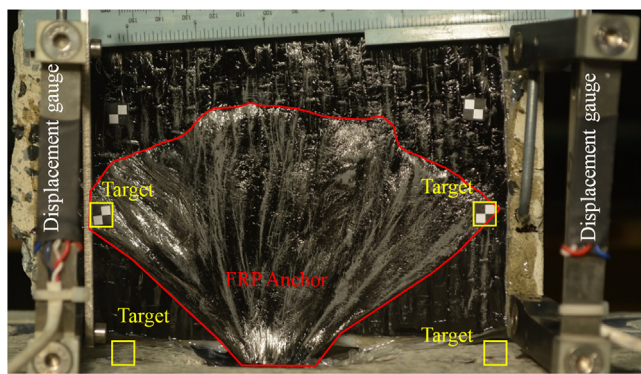


Fig. 7. DIC targets and displacement gauges in an FRP anchor specimen.

the use of foil strain gauges.

3. Discussion of results of DIC on FRP materials

Results from small scale FRP coupon tests, FRP anchors and FRP anchors installed on reinforced concrete columns are reported in this section. All full strain maps, both transverse and longitudinal, are scaled from -2% (compression) to $+2\%$ (tension).

3.1. FRP coupon testing

As discussed in Section 2.2 Test set up and methodology, FRP coupons were tested in accordance with the ASTM standards for tensile properties and for lap shear adhesive strength [58–60]. The DIC recordings for the tensile properties testing are reported first, while the DIC recordings for lap shear adhesive strength are reported at the end of this section.

The strain fields in the transverse (ϵ_t) direction are reported in

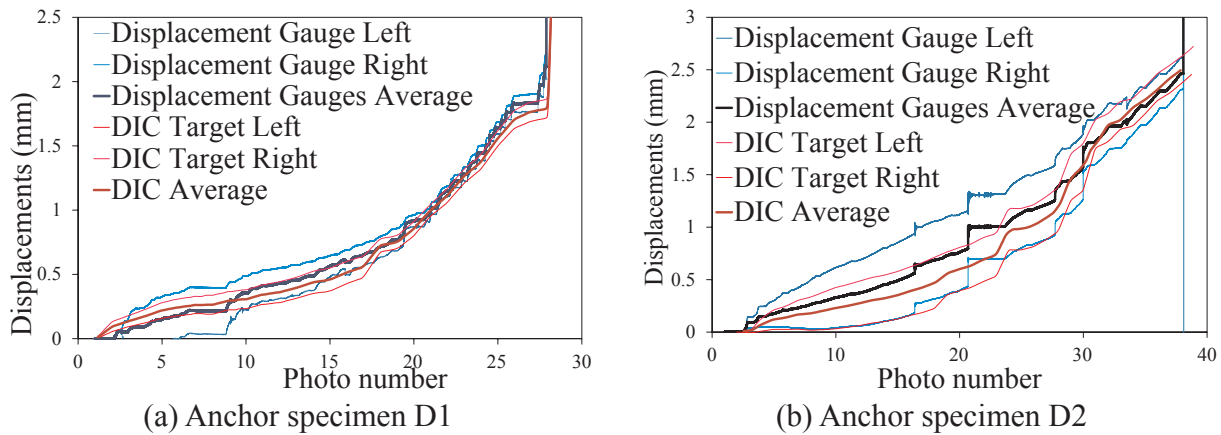


Fig. 8. Correlation of displacements when measured with DIC and displacement gauges.

Fig. 12 for 13 steps in the last two thirds of the test for specimen M2, previously used to validate the strains with SGs. The effect of the weave of the fabric on the strains can be seen in the transverse direction strain fields, which are patterned in phase with the weave of the tows. Typical Poisson’s ratios for FRP materials are between 0.2 and 0.35, such that for tension in the longitudinal direction it is expected that compression is developed in the transverse direction. However, the strain fields in Fig. 12 range from tension to compression. The likely source of this observation is the variation in properties between resin rich and fiber rich regions previously discussed. Although the out-of-plane movement of the FRP coupon was prevented during testing, it is possible that small amounts of out-of-plane deformation that may be misconstrued as in-plane strains were recorded as the fibers straightened from slack to taut under tension.

The strain fields in the longitudinal (ϵ_l) direction obtained while testing specimen M2 are reported in Fig. 13 for the same 13 steps than in Fig. 12, with the strains in the longitudinal direction linearly increasing as the load increased. The effect of the weave pattern on the strain fields can also be seen in Fig. 13, but the effect of the weave on the strain fields in the longitudinal direction is less significant than in the transverse direction. The magnitude of the recorded strains in the tows with the convex surface facing the cameras were higher than the magnitude of the strains in the tows with the concave surface facing the

cameras. This is due to the limitation of DIC to capture the strains only at the surface of the material, as discussed above. The resin in the part of the tows with the concave surface facing the cameras are more stretched than the resin in the part of the tows with the convex surface facing the cameras. Therefore, the resin in the concave parts experiences higher strains than the resin in the convex parts, although the fibers experience a consistent strain.

The strain patterns for the lap shear adhesive strength tests are reported in Fig. 14a for the direction transverse to the fibers and Fig. 14b for the direction longitudinal to the fibers, with the strain ranging from -2% in compression to $+2\%$ in tension. The strain patterns reported in Fig. 12 and Fig. 13 did not develop as strongly when the lap shear adhesive strength was being tested because the load at which debonding occurred was always lower than the load at which failure would occur. The strain levels were smaller in the region where the lap splice was located, as there are two times more material in this region than in the other regions. A concentration of strains in the longitudinal direction was observed at the end of lap region, where debonding would eventually occur. This behaviour was confirmed for all specimens, regardless of the bond length or bond area, which has been marked in Fig. 14. These results helped develop the lap shear strength predictive models reported in detail elsewhere [68].

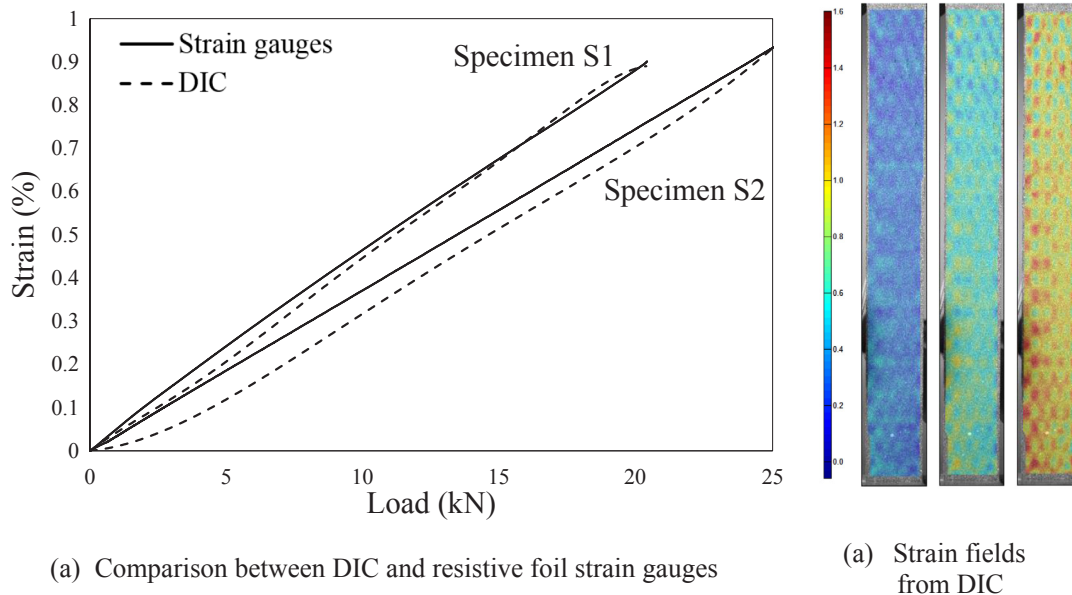


Fig. 9. Strain results for coupon specimens S1 and S2.

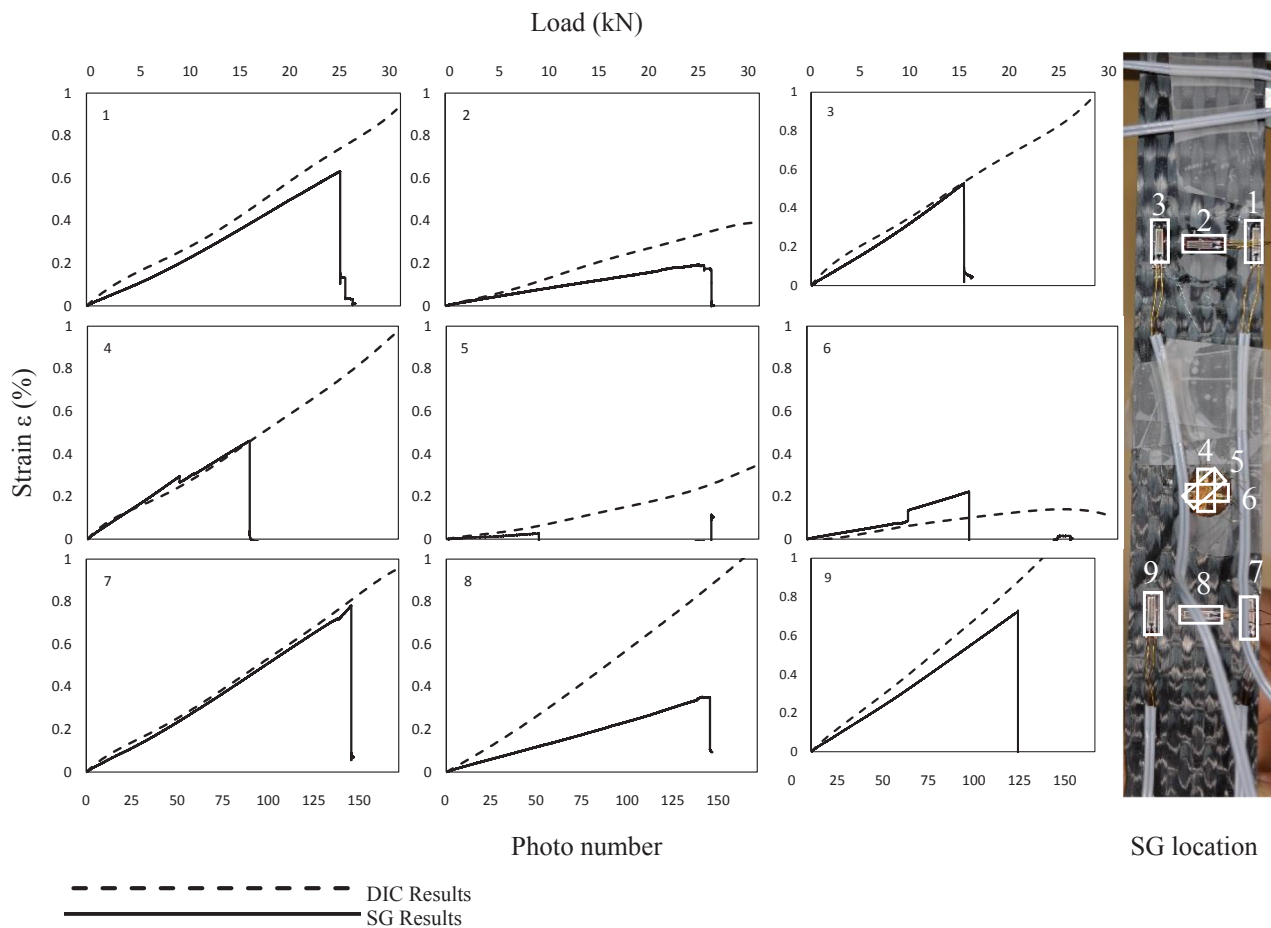


Fig. 10. Strain correlation for specimen M1.

3.2. FRP anchors testing

An extensive experimental program investigating the tensile capacity of straight and bent FRP anchors exhibiting fiber rupture failure was undertaken by the authors, further details on testing set-up and results were reported elsewhere [55,57]. DIC was used to capture full field strain maps, identify the failure mechanism and develop a design model that would be in accordance with the observations. Of all the DIC recordings captured during the testing, only three examples are reported herein due to space constraints.

The results from the first example, obtained while testing a narrow straight anchor (specimen A1), are reported in Figs. 15 and 16. The full field strain maps for transverse and longitudinal strains extracted from the last picture before failure, together with a picture of the failed anchor, are reported in Fig. 15. The longitudinal strain map featured a large concentration of tension strains (in red) at the bottom of the anchor, with the strain levels being close to the rupture strain (1.3%). The longitudinal strain in the FRP sheet, reported in Fig. 15a, remained close to zero because all the tension load was being transferred by the FRP anchor. DIC often derives in localized mistakes typically characterized by closely located tension and compression points, as identified by the red circles in Fig. 15a. The transverse strain map reported in Fig. 15b indicated how and where the failure was expected, with the large tension and compression shades being analogous to the fiber failure pattern outlined in yellow in Fig. 15c. This observation, which was common for almost all the measurements, indicated that the transverse strains had a large influence on the rupture of fiber rupture of FRP anchors. The elongated red shade on the left hand side of the anchor in Fig. 15b illustrates the tension forces between the sheet and the anchor as the FRP-to-FRP debonding force increased. The

development of the strain maps as the anchor was tested can be seen in the recordings reported in Fig. 16 for 1/3, 2/3 and at the end of the test. The development was linearly correlated to the increment in applied load.

Although the readings reported in Figs. 15 and 16 are representative of the most common behavior observed during testing, atypical results were also encountered. Two such examples are reported in Fig. 17, showing the strain maps corresponding to the last picture before rupture of two wide anchors (specimens A2 and A3). In the case of the wide bent anchor the sheet ruptured longitudinally at an early stage of the test, which can be observed in both the longitudinal and the transverse strain maps. The rupture of the sheet determined the way the anchor failed at the key portion at the bottom of the anchor but the failure load was not significantly different to the failure load of other anchors. The transverse strains map from the wide straight anchor is characterized by extreme tension strains on half of the anchor and extreme compression strains on the other half. This behavior is indicative that there was a slight misalignment between the point where the load was applied and the point where the anchor was introduced into the concrete substrate, which induced a rotation into the FRP sheet that was captured as tension/compression discrepancies in the transverse strains map reported in Fig. 17d. This slight rotation was not observed to affect the ultimate load at which the anchor failed when compared to anchors that failed in a more typical manner.

3.3. FRP anchors on RC columns

A total of five RC columns strengthened with FRP anchors were cyclically tested as part of a larger research project, with the FRP anchors being sandwiched between two layers of unidirectional FRP

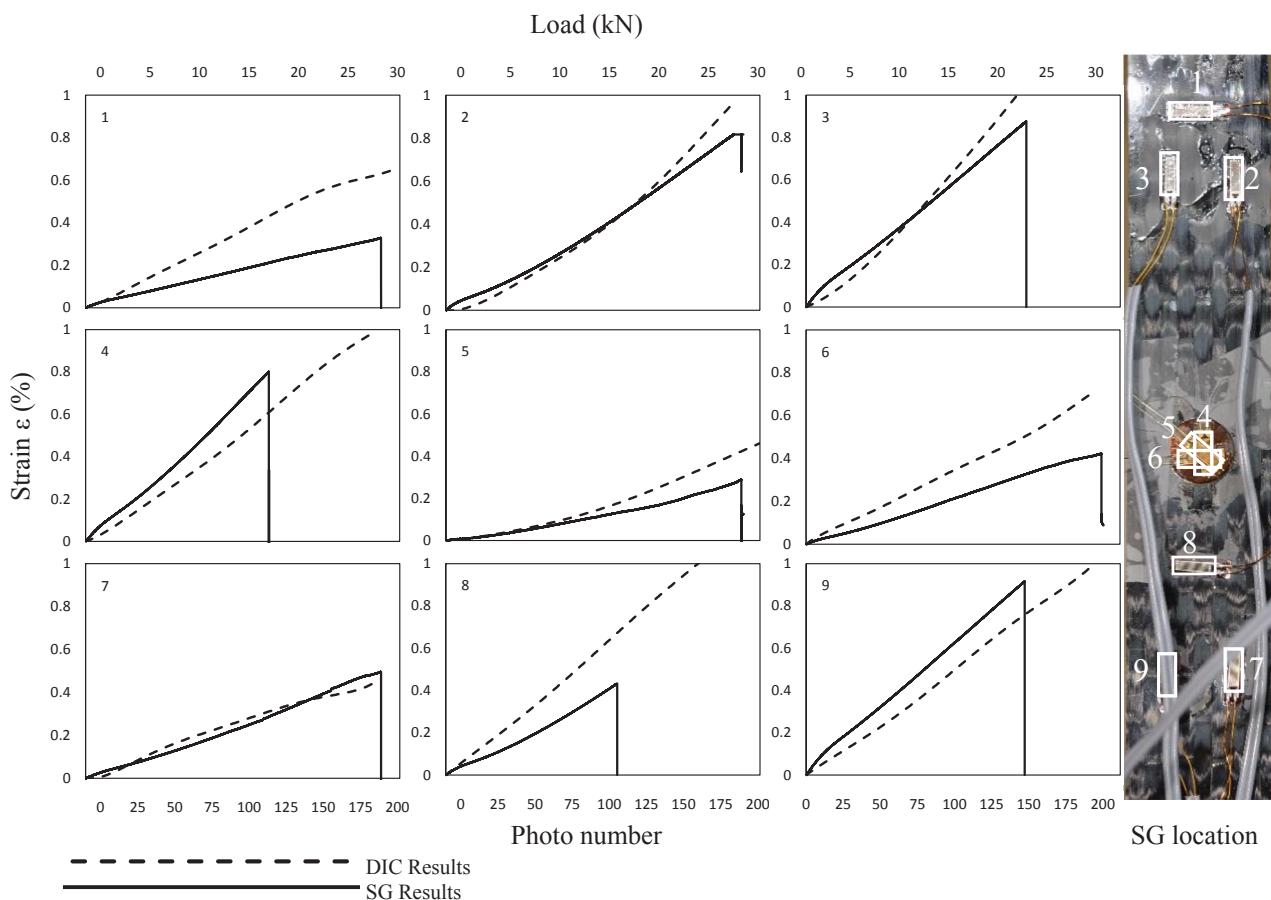


Fig. 11. Strain correlation for specimen M2.

sheets and installed onto the concrete surface, further details of the testing set-up and results were reported elsewhere [55]. Selected strain maps of one cycle of one of the columns (specimens C) are reported in Fig. 18, but the strain maps are representative of the results observed on

the other columns.

Similarly to the strain fields obtained with isolated FRP anchor testing, the longitudinal strain maps did not give conclusive insight to where and how the anchors ruptured. A large concentration of tensile

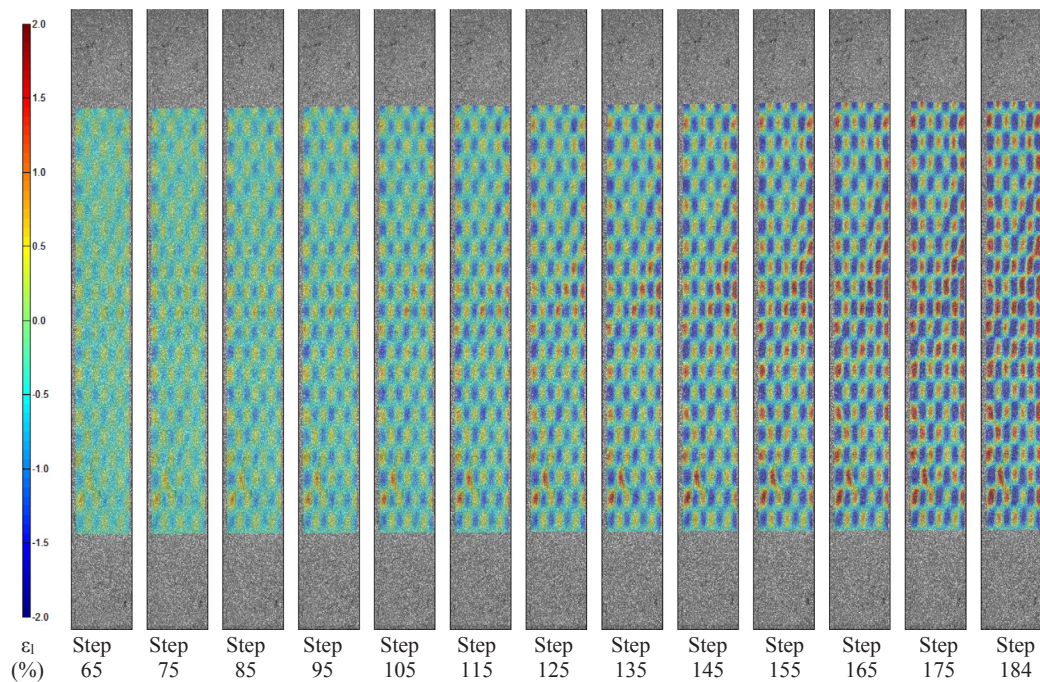


Fig. 12. Strains in the transverse direction for specimen M2.

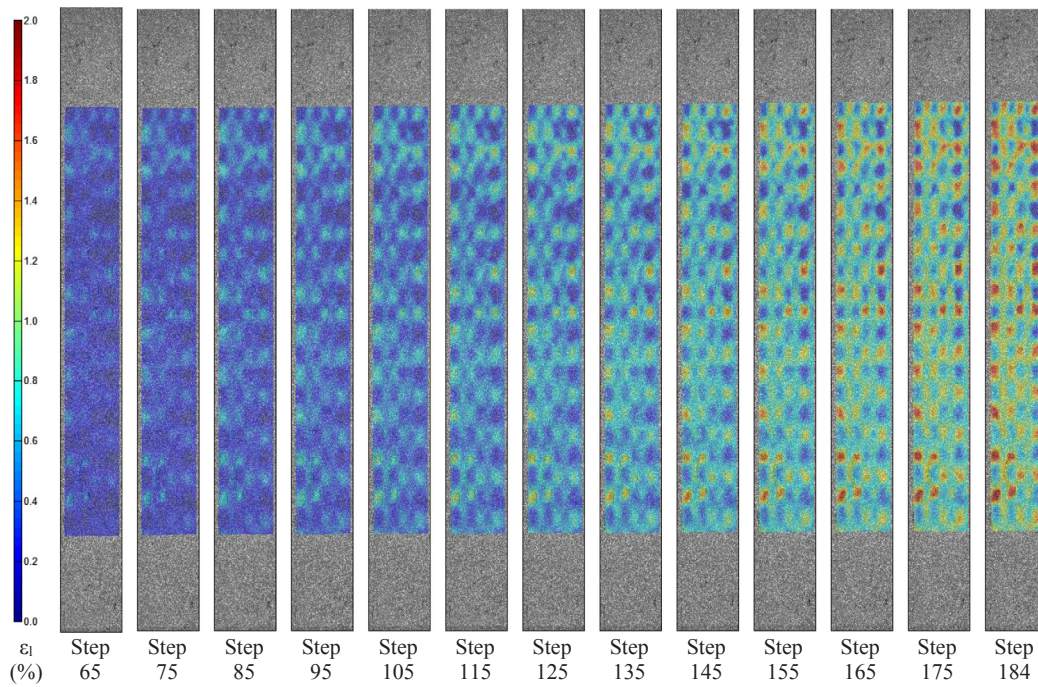


Fig. 13. Strains in the longitudinal direction for specimen M2.

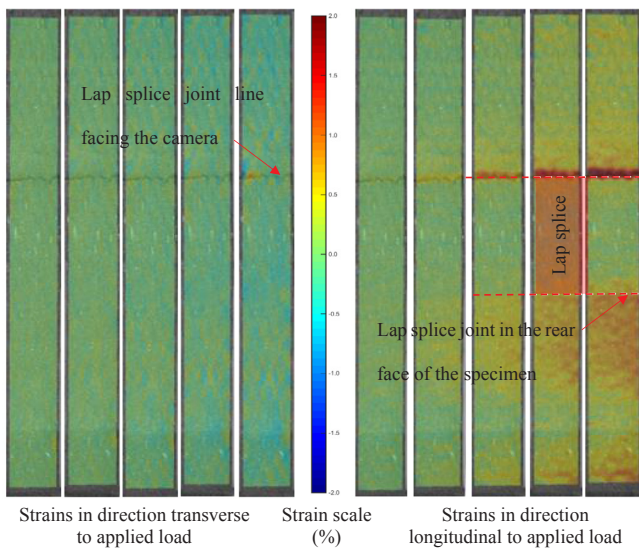


Fig. 14. Strain field in FRP coupons testing lap splice joints.

strains can be observed at the bottom of all three anchors, with the strain being higher on the right hand side anchor. This anchor was the first one to rupture, followed by the middle anchor and the anchor of the left hand side, probably due to eccentricities in construction and/or testing or material irregularities. However, when observing the transverse strain maps, only the anchor on the right hand side featured high tension/compression patterns like the patterns observed on isolated anchors and reported in Fig. 15. As in the case of isolated anchors, the transverse strain maps indicated which anchor failed and how. Large transverse tension strains were recorded on the sides of the three anchors, especially the left hand side anchor, which corresponded with the tensile strains on the FRP sheets covering the anchors as the sheets stretched. The small compression mark on the left hand side of the figure was originated from an undulation of the FRP sheet and was therefore not related to the anchor behavior.

4. Conclusions

The reported findings present the measurement of displacements and strains on FRP materials for use in civil engineering applications, where asymmetric, anisotropic and heterogeneous materials can be expected. Lens spherical aberration and image rectification errors were insignificant and can be disregarded when the cameras are used in a similar set-up as in this study (streamlining the process of obtaining displacements and strains with DIC). The correlation between the displacements measured with mechanical gauges and with DIC was generally satisfactory, but the correlation between the strains measured with foil strain gauges and with DIC depended on the direction in which the strains were measured. The correlation was coincident for strains measured in the direction parallel to the direction of the fibers, but the correlation was divergent for strains measured in any other direction.

Several examples were presented of the behavior of FRP materials based on the strain fields obtained with DIC. The results from the strain fields suggest that the strains in the transverse direction might have an equal or even larger influence on the strength and behavior of FRP materials than the strains in the longitudinal direction. Strain fields obtained using DIC were key in the study of the behavior of FRP materials.

The main findings resulting from the results have been summarized below:

- The optimum speckle pattern size must be between 3×3 and 4×4 pixel. The smallest deformation was observed when a focal length of 35 mm was used. The negligible reprojection error also indicated a good match between the mathematical camera model and the actual/physical camera behavior. The negligible reprojection error also indicated a good match between the mathematical camera model and the actual/physical camera behaviour.
- Although the use of specialised equipment will always be preferable, this equipment is typically expensive and complex to use. The use of commercially available and easy to use DSLR cameras gave accurate results both in terms of displacements and strains.
- DIC can capture multi-direction field strains of regions which are smaller than common strain gauges (i.e., 2 mm by 5 mm). The

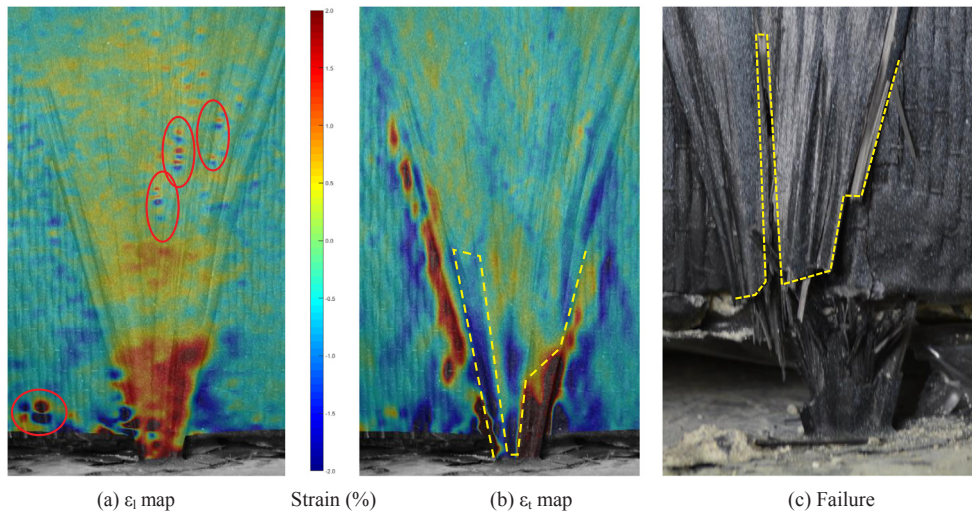


Fig. 15. DIC analysis and failure of a narrow straight anchor (A1) with $A_{dow} = 84 \text{ mm}^2$.

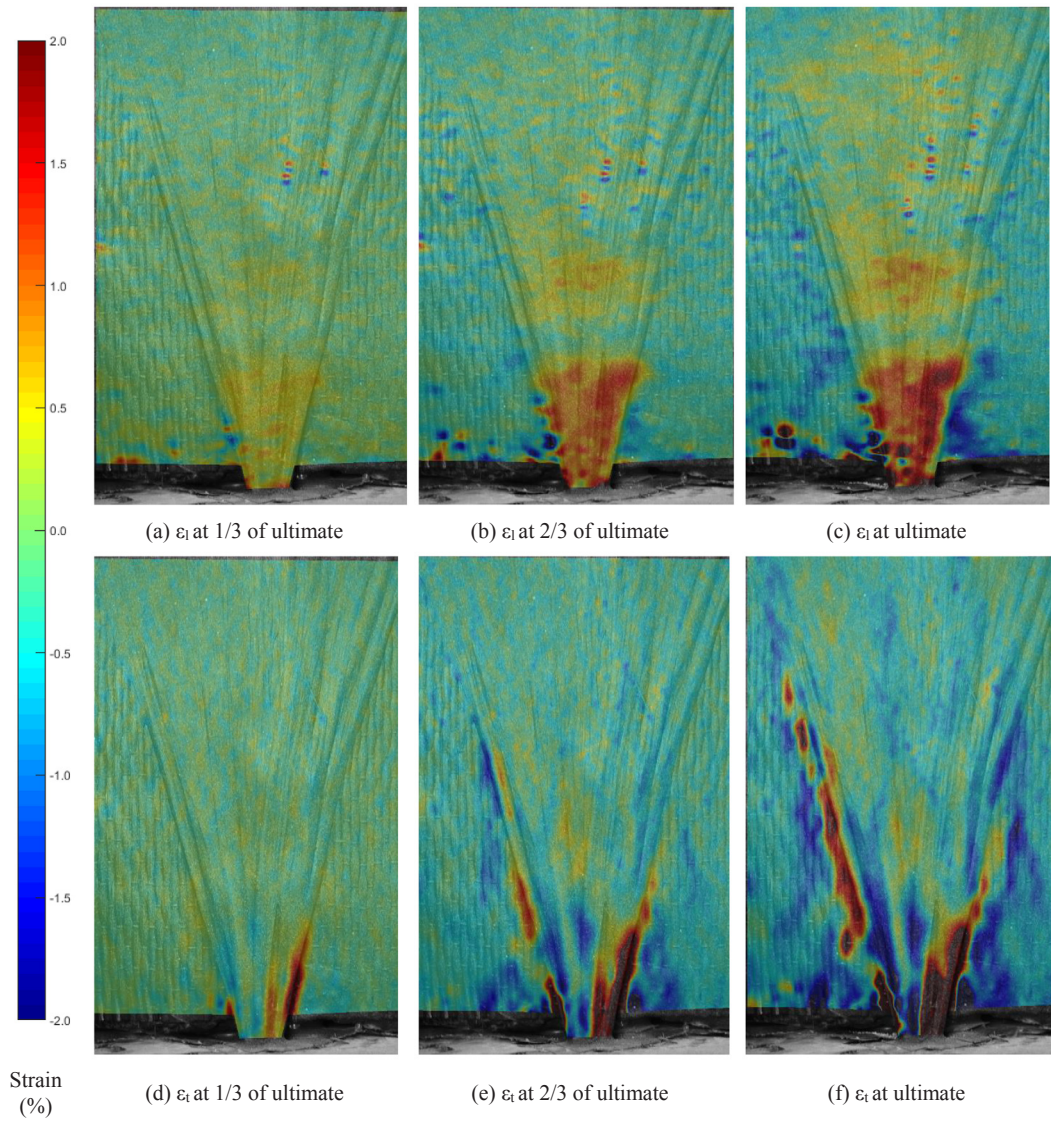


Fig. 16. Strain development when testing a narrow straight anchor (A1) with $A_{dow} = 84 \text{ mm}^2$.

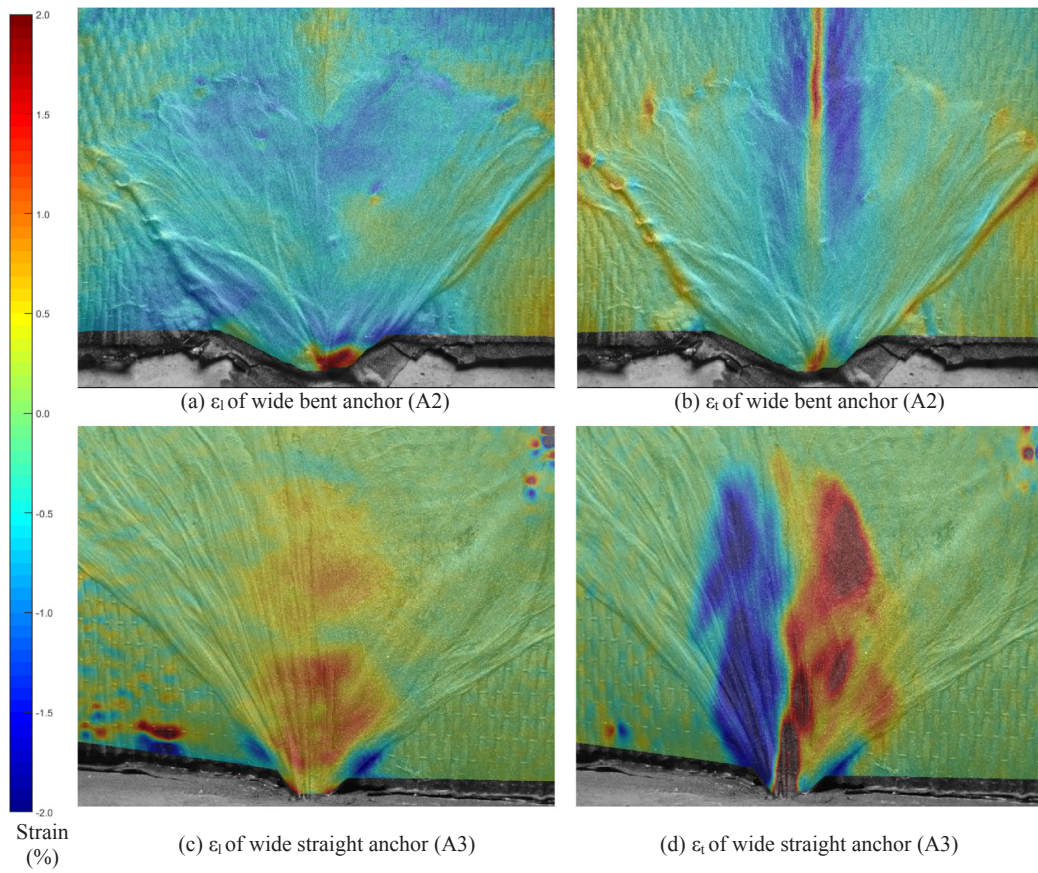


Fig. 17. Strain maps of particular cases of anchors.

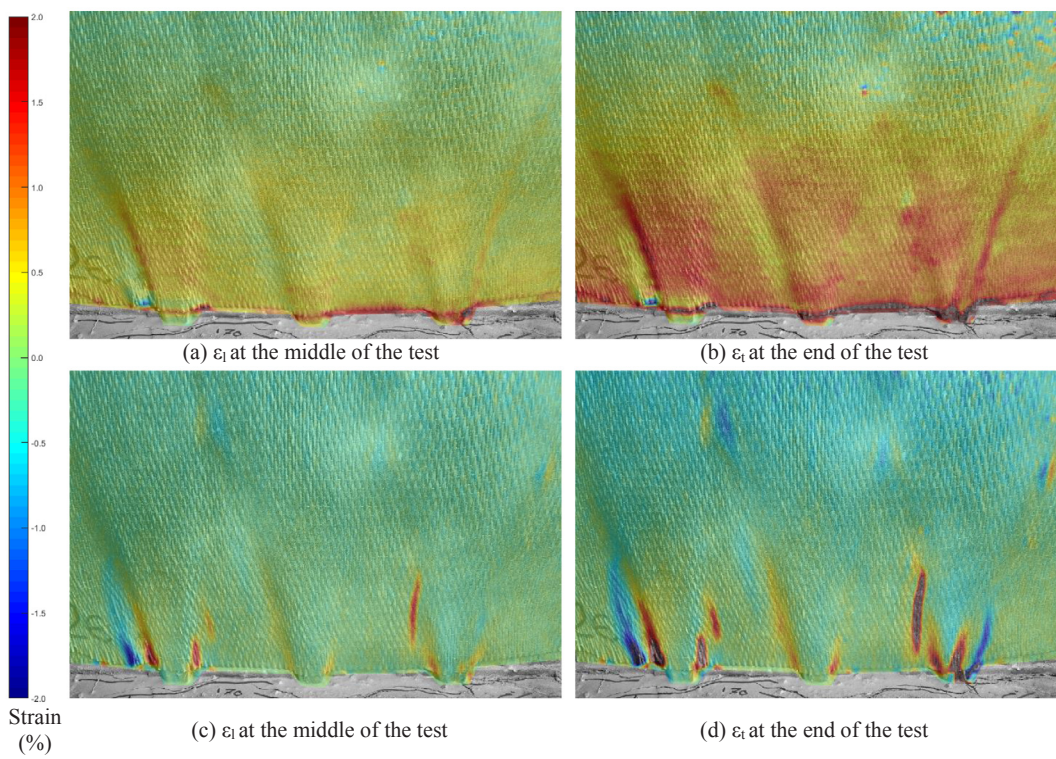


Fig. 18. DIC analysis of straight FRP anchors installed at the base of an RC column (C).

consistent measurement results showed the potential capability of measuring or observing the rupture strains of FRP materials and how the capacity is influenced by these strains. The measurement of debonding effects can also be improved using DIC, as opposed to strain gauges, given that the debonding line is thin and easy to misread.

- DIC enabled the capture of multi-direction field strains on FRP anchors, which would have been extremely difficult to obtain using traditional methods given the geometry of the anchors. The results obtained with DIC gave insight on how the stresses were distributed around the anchor, and how the stresses in the transverse direction had an effect on anchor capacity when fibre rupture was expected. Additionally, DIC helped detecting anomalies in some tests that would have otherwise evaded the results from traditional equipment, unless a very extensive, costly and time-consuming instrumentation campaign had been put in place.
- The use of DIC confirmed the damage observed in full-scale case study testing. This result could be used to be able to predict where the damage will occur before it actually happens.

Acknowledgments

The authors acknowledge the support of the technical staff of the Department of Civil and Environmental Engineering and of the Centre of Advanced Composite Materials at the University of Auckland. The materials used in this project were supplied by Contech Limited and Sika (NZ), and their contribution to the success of this project is gratefully acknowledged. Funding support provided by the New Zealand Earthquake Commission is highly appreciated. This project was (partially) supported by QuakeCoRE, a New Zealand Tertiary Education Commission-funded Centre.

References

- [1] ACI 440.2R. Guide for the design and construction of externally bonded FRP systems for strengthening concrete structures. Farming Hills Michigan, U.S.A.: American Concrete Institute (ACI) Committee 440; 2017. [https://doi.org/10.1061/40753\(171\)159](https://doi.org/10.1061/40753(171)159).
- [2] CNR-DT 200. Guide for the design and construction of externally bonded FRP systems for strengthening existing structures. Rome, Italy: CNR (Consiglio Nazionale delle Ricerche) – Advisory Committee on Technical Recommendations for Construction; 2013.
- [3] Stratford TJ, Bisby LA. Effect of warm temperatures on externally bonded FRP strengthening. *J Compos Constr* 2012;16(3):235–44. [https://doi.org/10.1061/\(ASCE\)CC.1943-5614.0000260](https://doi.org/10.1061/(ASCE)CC.1943-5614.0000260).
- [4] Tekieli M, De Santis S, de Felice G, Kwiecień A, Roscini F. Application of Digital Image Correlation to composite reinforcements testing. *Compos Struct* 2017;160:670–88. <https://doi.org/10.1016/j.compstruct.2016.10.096>. URL:<http://linkinghub.elsevier.com/retrieve/pii/S0263822316313915>.
- [5] Peters W, Ranson W. Digital imaging techniques in experimental stress analysis. *Opt Eng* 1982;21(3):213–427. <https://doi.org/10.1117/12.7972925>.
- [6] Chu TC, Ranson WF, Sutton MA. Applications of digital-image-correlation techniques to experimental mechanics. *Exp Mech* 1985;25(3):232–44. <https://doi.org/10.1007/BF02325092>.
- [7] Sutton MA, Yan JH, Tiwari V, Schreier HW, Orteu JJ. The effect of out-of-plane motion on 2D and 3D digital image correlation measurements. *Opt Lasers Eng* 2008;46(10):746–57. <https://doi.org/10.1016/j.optlaseng.2008.05.005>.
- [8] Gao Y, Cheng T, Su Y, Xu X, Zhang Y, Zhang Q. High-efficiency and high-accuracy digital image correlation for three-dimensional measurement. *Opt Lasers Eng* 2014;65:73–80. <https://doi.org/10.1016/j.optlaseng.2014.05.013>.
- [9] Broggiato GB, Newaz GM, Amodio D. Application of digital speckle correlation for strain measurement in composites. *Exp Tech Design Compos Mater* 2002;5(221):337–46. <https://doi.org/10.4028/www.scientific.net/KEM.221-222.337>.
- [10] Tao G, Xia Z. A non-contact real-time strain measurement and control system for multiaxial cyclic/fatigue tests of polymer materials by digital image correlation method. *Polym Testing* 2005;24(7):844–55. <https://doi.org/10.1016/j.polymertesting.2005.06.013>.
- [11] Hao W, Ge D, Ma Y, Yao X, Shi Y. Experimental investigation on deformation and strength of carbon/epoxy laminated curved beams. *Polym Testing* 2012;31(4):520–6. <https://doi.org/10.1016/j.polymertesting.2012.02.003>.
- [12] Namala KK, Mahajan P, Bhatnagar N. Digital image correlation of low velocity impact on glass/epoxy composite. *Int J Comput Methods Eng Sci Mech* 2014;15(3):203–17. <https://doi.org/10.1080/15502287.2014.882441>. URL:<http://www.tandfonline.com/doi/abs/10.1080/15502287.2014.882441>.
- [13] Tiwari V, Sutton MA, McNeill SR, Xu S, Deng X, Fournery WL, Bretall D. Application of 3D image correlation for full-field transient plate deformation measurements during blast loading. *Int J Impact Eng* 2009;36(6):862–74. <https://doi.org/10.1016/j.ijimpeng.2008.09.010>.
- [14] Pan B, Qian K, Xie H, Asundi A. Two-dimensional digital image correlation for in-plane displacement and strain measurement: a review. *Meas Sci Technol* 2009;20(6):062001. <https://doi.org/10.1088/0957-0233/20/6/062001>.
- [15] Yoneyama S, Kikuta H, Kitagawa A, Kitamura K. Lens distortion correction for digital image correlation by measuring rigid body displacement. *Opt Eng* 2006;45(2):023602. <https://doi.org/10.1117/1.2168411>.
- [16] Pan B, Yu L, Wu D, Tang L. Systematic errors in two-dimensional digital image correlation due to lens distortion. *Opt Lasers Eng* 2013;51(2):140–7. <https://doi.org/10.1016/j.optlaseng.2012.08.012>.
- [17] Lava P, Van Paeppegem W, Coppieters S, De Baere I, Wang Y, Debruyne D. Impact of lens distortions on strain measurements obtained with 2D digital image correlation. *Opt Lasers Eng* 2013;51(5):576–84. <https://doi.org/10.1016/j.optlaseng.2012.12.009>.
- [18] Kahn-Jetter ZL, Chu TC. *Exp Mech* 1990;30(1):10–6. <https://doi.org/10.1007/BF02322695>. URL:<http://link.springer.com/article/10.1007/BF02322695>.
- [19] Garcia D, Orteu JJ, Penazzi L. A combined temporal tracking and stereo-correlation technique for accurate measurement of 3D displacements: application to sheet metal forming. *J Mater Process Technol* 2002;125:736–42.
- [20] Fard M, Liu Y, Chattopadhyay A. Characterization of epoxy resin including strain rate effects using digital image correlation system. *J Aerospace Eng* 2011;25(2):308–19. [https://doi.org/10.1061/\(ASCE\)AS.1943-5525.0000127](https://doi.org/10.1061/(ASCE)AS.1943-5525.0000127). URL:[http://ascelibrary.org/doi/abs/10.1061/\(ASCE\)AS.1943-5525.0000127](http://ascelibrary.org/doi/abs/10.1061/(ASCE)AS.1943-5525.0000127).
- [21] Hung P-C, Voloshin AS. In-plane strain measurement by digital image correlation. *J Braz Soc Mech Sci Eng* 2003;25(3):215–21. <https://doi.org/10.1590/S1678-58782003000300001>.
- [22] Lee C, Take WA, Hout NA. Optimum accuracy of two-dimensional strain measurements using digital image correlation. *J Comput Civil* 2011;26(6):795–803. [https://doi.org/10.1061/\(ASCE\)CP.1943-5487.0000182](https://doi.org/10.1061/(ASCE)CP.1943-5487.0000182).
- [23] Hout NA, Andy Take W, Lee C, Dutton M. Experimental accuracy of two dimensional strain measurements using Digital Image Correlation. *Eng Struct* 2013;46:718–26. <https://doi.org/10.1016/j.engstruct.2012.08.018>.
- [24] Mehdikhani M, Aravand M, Sabuncuoğlu B, Callens MG, Lomov SV, Gorbatikh L. Full-field strain measurements at the micro-scale in fiber-reinforced composites using digital image correlation. *Compos Struct* 2016;140:192–201. <https://doi.org/10.1016/j.compstruct.2015.12.020>. URL:<http://www.sciencedirect.com/science/article/pii/S0263822315011101>.
- [25] Lecomte D, Smits A, Bossuyt S, Sol H, Vantomme J, Van Hemelrijck D, Habraken AM. Quality assessment of speckle patterns for digital image correlation. *Opt Lasers Eng* 2006;44(11):1132–45. <https://doi.org/10.1016/j.optlaseng.2005.10.004>.
- [26] Yamaguchi T, Nakamura S, Saegusa R, Hashimoto S. Image-based crack detection for real concrete surfaces. *IEEJ Trans Electr Electron Eng* 2008;3(1):128–35. <https://doi.org/10.1002/tee.20244>.
- [27] Yang Y-S, Huang C-W, Wu C-L. A simple image-based strain measurement method for measuring the strain fields in an RC-wall experiment. *Earthq Eng Struct Dyn* 2012;41(1):1–17. <https://doi.org/10.1002/eqe>. URL:[http://www.stanford.edu/bakerjw/Publications/Baker \(2007\) Record scaling, SPCEE.pdf?%2Fpublication%2Fuid%2F1498A307-A88B-4AAF-B3F7-E6B4B14F87C2](http://www.stanford.edu/bakerjw/Publications/Baker%20(2007)%20Record%20scaling,%20SPCEE.pdf?%2Fpublication%2Fuid%2F1498A307-A88B-4AAF-B3F7-E6B4B14F87C2).
- [28] Dutton M, Take WA, Hout NA, Asce M. Curvature monitoring of beams using digital image correlation. *J Bridge Eng* 2013;19(3):05013001. [https://doi.org/10.1061/\(ASCE\)BE.1943-5592.0000538](https://doi.org/10.1061/(ASCE)BE.1943-5592.0000538).
- [29] Ghorbani R, Matta F, Sutton M. Full-field deformation measurement and crack mapping on confined masonry walls using digital image correlation. *Exp Mech* 2015;55(1):227–43. <https://doi.org/10.1007/s11340-014-9906-y>. URL:<http://link.springer.com/10.1007/s11340-014-9906-y>.
- [30] Czaderski C, Motavalli M. Continuous slip measurements on an EBR strengthened RC beam. Proceedings of the Fourth International Conference on FRP composites in Civil Engineering (CICE), Zurich, Switzerland. 2008.
- [31] Czaderski C, Soudki K, Motavalli M. Front and side view image correlation measurements on FRP to concrete pull-off bond tests. *J Compos Constr* 2010;14(4):451–63. [https://doi.org/10.1061/\(ASCE\)CC.1943-5614.0000106](https://doi.org/10.1061/(ASCE)CC.1943-5614.0000106).
- [32] Ghiassi B, Xavier J, Oliveira DV, Lourenço PB. Application of digital image correlation in investigating the bond between FRP and masonry. *Compos Struct* 2013;106:340–9. <https://doi.org/10.1016/j.compstruct.2013.06.024>.
- [33] Caggegi C, Chevalier L, Pensée V, Cuomo M. Strain and shear stress fields analysis by means of Digital Image Correlation on CFRP to brick bonded joints fastened by fiber anchors. *Constr Build Mater* 2016;106:78–88. <https://doi.org/10.1016/j.conbuildmat.2015.12.089>.
- [34] Barrington J, Dickson D, Bisby L, Stratford T. Strain development and hoop strain efficiency in FRP confined square columns. *ACI Spec Publ* 2011;275:1–20.
- [35] Bisby LA, Chen JF, Li SQ, Stratford TJ, Cueva N, Crossling K. Strengthening fire-damaged concrete by confinement with fibre-reinforced polymer wraps. *Eng Struct* 2011;33(12):3381–91. <https://doi.org/10.1016/j.engstruct.2011.07.002>.
- [36] Périé J-N, Calloch S, Cluzel C, Hild F. Analysis of a multiaxial test on a C/C composite by using digital image correlation and a damage model. *Exp Mech* 2002;42(3):318–28. <https://doi.org/10.1007/BF02410989>.
- [37] Yao W, Li J, Wu K. Mechanical properties of hybrid fiber-reinforced concrete at low fiber volume fraction. *Cem Concr Res* 2003;33(1):27–30. [https://doi.org/10.1016/S0008-8846\(02\)00913-4](https://doi.org/10.1016/S0008-8846(02)00913-4).
- [38] Meng LB, Jin GC, Yao XF, Yeh HY. 3D full-field deformation monitoring of fiber composite pressure vessel using 3D digital speckle correlation method. *Polym Testing* 2006;25(1):42–8. <https://doi.org/10.1016/j.polymertesting.2005.09.011>.
- [39] Ivanov D, Ivanov S, Lomov S, Verpoest I. Strain mapping analysis of textile

- composites. *Opt Lasers Eng* 2009;47(3):360–70. <https://doi.org/10.1016/j.optlaseng.2008.05.013>.
- [40] Brynk T, Molak RM, Janiszewska M, Pakiela Z. Digital Image Correlation measurements as a tool of composites deformation description. *Comput Mater Sci* 2012;64:157–61. <https://doi.org/10.1016/j.commatsci.2012.04.034>.
- [41] Kiasat MS, Sangtabi MR. Effects of fiber bundle size and weave density on stiffness degradation and final failure of fabric laminates. *Compos Sci Technol* 2015;111:23–31. <https://doi.org/10.1016/j.compscitech.2015.02.016>.
- [42] Kwon J, Choi J, Huh H, Lee J. Evaluation of the effect of the strain rate on the tensile properties of carbon-epoxy composite laminates. *J Compos Mater* 2016. <https://doi.org/10.1177/0021998316683439>. 0021998316683439.
- [43] Pohoryles DA, Melo J, Rossetto T, Fabian M, Mccague C, Stavrianaki K, Lishman B, Sargeant B, et al. Use of DIC and AE for monitoring effective strain and debonding in FRP and FRCM-retrofitted RC beams. *J Compos Constr* 2017;21(1). [https://doi.org/10.1061/\(ASCE\)CC.1943-5614.0000715](https://doi.org/10.1061/(ASCE)CC.1943-5614.0000715).
- [44] Sutton MA, Zhao W, McNeill S, Helm J, Riddell W, Piascik R. Local crack closure measurement system using computer vision and a far-field microscope, ASTM STP 1343 on crack closure measurements. K. Smith and J. McDowell; 1999.
- [45] Yao XF, Meng LB, Jin JC, Yeh HY. Full-field deformation measurement of fiber composite pressure vessel using digital speckle correlation method. *Polym Testing* 2005;24(2):245–51. <https://doi.org/10.1016/j.polymertesting.2004.05.009>.
- [46] Bisby LA, Take WA. Strain localisations in FRP-confined concrete: new insights. *Proc Inst Civil Eng* 2009;162(5):301–9. <https://doi.org/10.1680/stbu.2009.162.5.301>. URL:<http://www.scopus.com/inward/record.url?eid=2-s2.0-77955786033&partnerID=40&md5=936df57365ddc926d81324de73d129bd>.
- [47] Kim S, Smith S. Behaviour of handmade FRP anchors under tensile load in uncracked concrete. *Adv Struct Eng* 2009;12(6):845–65. <https://doi.org/10.1260/136943309790327716>.
- [48] del Rey Castillo E, Rogers R, Griffith MC, Ingham JM. Tensile strength of straight Frp anchors in Rc structures. Proceedings of The 12th International Symposium on Fiber Reinforced Polymers for Reinforced Concrete Structures (FRPRCS-12) & The 5th Asia-Pacific Conference on Fiber Reinforced Polymers in Structures (APFIS-2015) Joint Conference, no. December, Nanjing, China. 2015.
- [49] del Rey Castillo E, Griffith MC, Ingham JM. Fibre rupture tensile capacity of FRP straight anchors. Proceedings of The New Zealand Concrete Industry Conference. Auckland, New Zealand: The New Zealand Concrete Society (NZCS); 2016.
- [50] del Rey Castillo E, Griffith M, Ingham JM. Force-based model for straight FRP anchors exhibiting fibre rupture failure mode. Proceedings of The 8th International Conference on Fibre-Reinforced Polymer (FRP) Composites in Civil Engineering (CICE 2016). Hong Kong, China: The Hong Kong Polytechnic University; 2016.
- [51] Lim J, Kim J, del Rey Castillo E, Griffith MC, Dizhur D, Ingham JM. Characterization of bent fibre reinforced polymer (FRP) anchors exhibiting fibre rupture failure mode. Proceedings of The New Zealand Concrete Industry Conference. Auckland, New Zealand: The New Zealand Concrete Society (NZCS); 2016.
- [52] del Rey Castillo E, Ingham J, Griffith M. Seismic strengthening of RC columns with straight FRP anchors. Proceedings of the 13th conference on Fiber Reinforced Polymers in Reinforced Concrete Structures (FRPRCS-13). Anaheim, California, USA: American Concrete Institute (ACI); 2017.
- [53] del Rey Castillo E, Ingham JM, Smith ST, Kanitkar R, Griffith MC. A design approach for FRP anchors in FRP-strengthened RC structures. Proceedings of the 13th conference on Fiber Reinforced Polymers in Reinforced Concrete Structures (FRPRCS-13). Anaheim, California, USA: American Concrete Institute (ACI); 2017.
- [54] del Rey Castillo E, Griffith M, Ingham J. Seismic behavior of RC columns flexurally strengthened with FRP sheets and FRP anchors. *Compos Struct* 2018;203:382–95. <https://doi.org/10.1016/j.compstruct.2018.07.029>.
- [55] del Rey Castillo E, Griffith MC, Ingham JM. Straight FRP anchors exhibiting fiber rupture failure mode. *Compos Struct* 2019;207:612–24. <https://doi.org/10.1016/j.compstruct.2018.09.073>.
- [56] del Rey Castillo E, Dizhur D, Griffith MC, Ingham JM. Strengthening RC structures using FRP spike anchors in combination with EBR systems. *Compos Struct*. <https://doi.org/10.1016/j.compstruct.2018.10.093>.
- [57] del Rey Castillo E, Griffith MC, Ingham JM. Experimental testing and design model for bent FRP anchors exhibiting fiber rupture failure mode. *Compos Struct*. <https://doi.org/10.1016/j.compstruct.2018.11.091>.
- [58] ASTM D3039. Standard test method for tensile properties of polymer matrix composite materials. West Conshohocken, Pennsylvania: American Society for Testing and Materials (ASTM); 2014. <https://doi.org/10.1520/D3039.D3039M-14>.
- [59] ASTM D5868. Standard test method for lap shear adhesion for fiber reinforced plastic (FRP). American Society for Testing and Materials (ASTM) 2014. <https://doi.org/10.1520/D5868-01R14.2>.
- [60] ASTM D3528. Standard test method for strength properties of double lap shear adhesive joints by. American Society for Testing and Materials (ASTM) 2016. <https://doi.org/10.1520/D3528-96R16.2>.
- [61] del Rey Castillo E, Griffith MC, Ingham JM. FRP anchors attributes. University of Auckland. 2017. <https://doi.org/10.17608/k6.auckland.5188456>.
- [62] Carter J, Uchic M, Mills M. Impact of Speckle Pattern Parameters on DIC Strain Resolution Calculated from In-situ SEM Experiments. Fracture, fatigue, failure, and damage evolution Springer International Publishing; 2015. p. 119–26. https://doi.org/10.1007/978-3-319-06977-7_vol_5.
- [63] MATLAB. MATLAB and statistics toolbox release 2015. Natick, Massachusetts, United States: The MathWorks Inc.; 2015.
- [64] Stubbing RM. Characterisation of polymeric foam cores using digital image correlation [Ph.D. thesis]. The University of Auckland, Department of Mechanical Engineering; 2013.
- [65] Stubbing RM. DTA report 408/NR 1690-digital image correlation capability. Auckland, New Zealand: Defence Technology Agency (DTA), New Zealand Defence Force; 2016.
- [66] Bouguet J-Y. Camera Calibration Toolbox for MATLAB; 2008. Available from: http://www.vision.caltech.edu/bouguetj/calib_doc/index.html.
- [67] Heikkilä J, Silvén O. A four-step camera calibration procedure with implicit image correction. Proceedings of the IEEE Computational Society Conference in Computer Vision and Pattern Recognition (CVPR'97). College Park, MD, USA: IEEE Xplore; 1997. p. 1106–12.
- [68] Singh A, del Rey Castillo E, Ingham JM. FRP-to-FRP bond characterization and force-based bond length model. *Compos Struct* (under review).